International Journal for Rapid Research in Engineering Technology & Applied Science (IJRRETAS)

(Peer-Reviewed, Open Access, Fully Refereed International Journal)

Volume 12 issue 02 February 2026 OPEN ACCESS E-ISSN: 2455-4723 Impact Factor 7.95

# Geospatial Assessment of Urban Expansion and Land Use/Land Cover Change in Jamshedpur, India

**Sadhna Kumari**

Research Scholar, Department of Geography, Amaltas University, Dewas

**Dr. Virendra Kumar**

Supervisor, Department of Geography, Amaltas University, Dewas

**Abstract**

Medium-sized industrial cities account for a growing share of Indian urbanisation, yet their land transformation remains poorly documented. This study assesses urban expansion and land use/land cover (LULC) change in Jamshedpur, Jharkhand, over a fixed 250 km² extent between 2000 and 2024. Landsat TM, ETM+, OLI and OLI-2 imagery for 2000, 2010, 2020 and 2024 was classified into five classes using the maximum likelihood classifier, and the results were evaluated through error matrices and the Kappa coefficient. Post-classification comparison, land consumption indicators, Shannon's entropy, proximity analysis, the Normalised Difference Vegetation Index (NDVI), land surface temperature (LST) and a CA-Markov model were used to examine the extent, pattern, consequences and future trajectory of growth. Overall accuracy rose from 86.80% to 92.40%, with Kappa values between 0.825 and 0.896. Built-up land expanded from 38.75 km² to 100.50 km² (159.35%), while agricultural land, vegetation and water bodies declined by 39.88%, 33.31% and 26.40%, respectively. About three-quarters of new built-up land was drawn directly from agricultural and vegetated land. Relative entropy increased from 0.9843 to 0.9918, the land consumption rate rose from 35.17 to 57.35 m² per person, and growth beyond 8 km from the centre exceeded 500%, indicating dispersed peripheral expansion. Mean NDVI fell by 34.95%, and urban heat island intensity rose from 5.10 °C to 7.40 °C. Under a business-as-usual scenario, built-up land would occupy 55.02% of the area by 2040. The findings call for density-oriented planning, protection of agricultural land and small water bodies, and deliberate sequencing of infrastructure.

**Keywords:** Urban expansion; land use/land cover change; remote sensing; GIS; Shannon's entropy; land surface temperature; CA-Markov; Jamshedpur

## 1. Introduction

### 1.1 Urban Growth in the Indian Context

India is in the middle of a long urban transition. Cities are absorbing an increasing share of the national population and economic activity, and their physical footprint is growing even faster than their populations. Much of the research on this transition has concentrated on metropolitan regions such as Delhi, Bengaluru and Chennai, where satellite-based studies have documented rapid paving of land and the loss of lakes, farmland and green spaces (Aithal & Ramachandra, 2016; Ramachandra et al., 2015; Tripathy & Kumar, 2019). Medium-sized cities have received less attention, although they are now among the fastest-growing urban places in the country

and are expanding in a manner that is frequently dispersed and weakly regulated (Chettry & Surawar, 2021).

### 1.2 Industrial Cities and Land Transformation

Industrial cities occupy a distinct position within this transition. Their growth is driven by a clearly identifiable economic engine, and industrial expansion generates employment, migration, housing demand and supporting infrastructure that together reshape the surrounding countryside. In eastern India, mineral-based industrial regions such as Asansol–Durgapur show how industry, mining and settlement combine to alter land cover and raise surface temperatures (Choudhury et al., 2019). Similar processes are visible in the state capital of Jharkhand, Ranchi, where built-up land has expanded rapidly into agricultural and open land (Ahmad & Goparaju, 2016). Understanding how such cities grow is essential if the economic benefits of industrialisation are to be reconciled with the protection of land, water and ecological resources.

### 1.3 Jamshedpur: Setting and Urban Character

Jamshedpur, in the East Singhbhum district of Jharkhand, was established in the early twentieth century as a planned company town around an integrated steel works and is widely known as the Steel City of India. It lies on the north-eastern margin of the Chota Nagpur plateau near the confluence of the Subarnarekha and Kharkai rivers, with the forested Dalma hills to the north. The urban agglomeration is administratively divided among the Jamshedpur and Mango Notified Area Committees, Jugsalai Municipality and the Adityapur Municipal Corporation, and its settlement geography is polycentric rather than concentric. The planned township with its green belts contrasts sharply with the informal growth of its fringes, and research on the adjoining Dalma Wildlife Sanctuary has already recorded steady losses of dense forest to settlement and bare land (Ranjan et al., 2016). A city-wide, multi-decadal assessment of land change, however, has been lacking.

### 1.4 Geospatial Technology for Land Change Monitoring

Remote sensing and geographic information systems (GIS) offer the most practical means of reconstructing land change over several decades. The free Landsat archive provides consistent 30 m multispectral observations from the 1980s onwards, and GIS supports overlay analysis, spatial metrics and modelling (Phiri & Morgenroth, 2017). Advances in classification algorithms, cloud processing platforms and artificial intelligence continue to expand these capabilities (Gorelick et al., 2017; Gu & Zeng, 2024; Talukdar et al., 2020). Together, these tools allow analysts to measure not only how much land has changed, but also where, in what form and with what environmental consequences.

### 1.5 Environmental Significance of Land Use Change

The replacement of vegetation, cropland and water with impervious surfaces alters runoff, groundwater recharge, habitat connectivity and local climate. Impervious surfaces absorb and re-emit more heat than vegetated or wet surfaces, which intensifies the surface urban heat island (Mathew et al., 2016; Pal & Ziaul, 2017). For an industrial city where heavy industry, dense settlement, forested hills and rivers sit in close proximity, these effects carry direct implications

for public health, flood exposure and long-term sustainability. This paper therefore presents an integrated geospatial assessment of urban expansion and LULC change in Jamshedpur from 2000 to 2024, combining classification, change detection, growth metrics, environmental indicators and predictive modelling.

## 2. Literature Review

### 2.1 Remote Sensing Data and Classification Approaches

Most Indian urban LULC studies rely on multi-temporal Landsat imagery because of its long archive, free access and consistent resolution, supplemented by higher-resolution imagery for training and validation (Bhat et al., 2017; Phiri & Morgenroth, 2017). In the Jamshedpur region, Ranjan et al. (2016) combined high-resolution imagery, GIS and GPS to track forest density change in Dalma between 2009 and 2016, reporting classification accuracy of about 95% and an annual loss of roughly 1.77 km² of very dense forest. Supervised classification with the maximum likelihood classifier has been the dominant method in Indian studies, including those of Dehradun, English Bazar and Asansol–Durgapur (Bhat et al., 2017; Choudhury et al., 2019; Pal & Ziaul, 2017).

Machine learning classifiers have gained ground because they make no assumption of normally distributed data. Belgiu and Drăguţ (2016) showed that random forest is robust and accurate across many remote sensing applications, and Talukdar et al. (2020) found that random forest and support vector machines generally outperform conventional methods, although their performance depends on training data and parameter tuning. Phiri and Morgenroth (2017) noted that the field has moved towards object-based and machine learning approaches, while Gu and Zeng (2024) highlighted the emerging role of deep learning in automated change detection. For long multi-sensor time series, however, consistency between dates remains as important as absolute accuracy, and a fully specified parametric classifier remains defensible.

### 2.2 Urban Sprawl Measurement and Growth Modelling

A rich set of indicators has been developed to describe the form of urban growth. Shannon's entropy is widely used to test whether built-up land is concentrated or dispersed; Bhat et al. (2017) applied it to Dehradun and found increasing dispersal, and Chettry and Surawar (2021) combined entropy with landscape metrics to show that sprawl is common across eight medium-sized Indian cities. Aithal and Ramachandra (2016) used a gradient-directional approach to show corridor-led, fragmented growth in Chennai, and Ramachandra et al. (2015) linked the rapid growth of Bengaluru to the loss of lakes and vegetation. Land consumption and absorption measures complement these spatial metrics by relating land change to population growth.

Predictive models extend this analysis into the future. Cellular automata and Markov chain models use observed transitions together with driving factors such as road proximity, slope and existing settlement to simulate growth. Tripathy and Kumar (2019) modelled the expansion of Delhi using cellular automata, Mishra and Rai (2016) combined a multi-layer perceptron with Markov chain analysis to project LULC change in Patna, and Hasnine and Rukhsana (2020)

integrated sprawl analysis with prediction of future urban areas. These methods have not previously been applied at city scale to Jamshedpur.

### 2.3 Land Use Change and the Urban Thermal Environment

A substantial literature links LULC change to land surface temperature. In Asansol–Durgapur, Choudhury et al. (2019) reported that industrial, mining and impervious surfaces were the hottest land covers, reaching around 38 °C against about 27 °C for vegetation and water. Pal and Ziaul (2017) observed a close association between built-up growth and rising LST in English Bazar, and Mathew et al. (2016) showed for Chandigarh that the proportion of impervious surface strongly controls surface temperature. Spectral indices are commonly used to explain these patterns: NDVI is generally negatively and the normalised difference built-up index positively related to LST (Mondal et al., 2021; Pandey et al., 2024). Methodological comparisons of retrieval algorithms have helped to standardise LST estimation in Indian settings (Sahana et al., 2016). Despite this body of work, no study has jointly examined urban expansion, sprawl, vegetation condition and surface temperature for Jamshedpur over a multi-decadal period, which this paper seeks to address.

## 3. Research Methodology

### 3.1 Study Area

The study area is a fixed rectangular extent of 250.00 km² (approximately 22.73°–22.87° N and 86.12°–86.28° E) centred on the Jamshedpur urban agglomeration and projected to UTM Zone 45N (WGS 1984). A geometric extent was preferred to administrative boundaries because the agglomeration spans several local bodies and two districts, boundaries have changed during the study period, and the most dynamic growth occurs beyond municipal limits. Elevation ranges from about 120 m along the rivers to just over 230 m on residual hills. The climate is tropical wet and dry, with about 1,400 mm of mean annual rainfall concentrated in the south-west monsoon.

### 3.2 Data Sources and Pre-processing

Four Landsat Level-1 scenes (path 140, row 045) were obtained from the USGS EarthExplorer archive for 2000, 2010, 2020 and 2024 (Table 1). All scenes were acquired between late November and mid-December to ensure phenological consistency and minimal cloud cover. Ancillary data comprised Survey of India 1:50,000 topographic sheets, SRTM one arc-second elevation data, high-resolution Google Earth and Sentinel-2 imagery for reference, and census-based population figures for 2001 and 2011, projected for 2020 and 2024. Scan-line gaps in the 2010 ETM+ scene were filled by local histogram matching. Pre-processing included image-to-image registration (RMSE below half a pixel), radiometric calibration to top-of-atmosphere reflectance, dark object subtraction for atmospheric correction, cross-sensor harmonisation of OLI reflectance to TM spectral space, and clipping to the study extent.

International Journal for Rapid Research in Engineering Technology & Applied Science (IJRRETAS)

(Peer-Reviewed, Open Access, Fully Refereed International Journal)

Volume 12 issue 02 February 2026 OPEN ACCESS E-ISSN: 2455-4723 Impact Factor 7.95

**Table 1: Satellite data used in the study**

| Year | Satellite / Sensor | Acquisition Date | Resolution (m) | Bands Used | Cloud (%) |
|---|---|---|---|---|---|
| 2000 | Landsat 5 TM | 14 Dec 2000 | 30 | 1–5, 7 | 1.24 |
| 2010 | Landsat 7 ETM+ | 22 Nov 2010 | 30 | 1–5, 7 | 0.86 |
| 2020 | Landsat 8 OLI/TIRS | 09 Dec 2020 | 30 | 2–7 | 0.42 |
| 2024 | Landsat 9 OLI-2/TIRS-2 | 03 Dec 2024 | 30 | 2–7 | 0.31 |

### 3.3 Classification and Accuracy Assessment

Each image was classified into five classes (built-up, vegetation, agricultural land, water bodies and barren/open land) using a modified Anderson Level I scheme and the maximum likelihood classifier with equal prior probabilities. Between 74 and 204 training polygons per class per year were digitised over homogeneous areas, and transformed divergence values above 1,750 for all class pairs confirmed adequate spectral separability. A 3 × 3 majority filter and a minimum mapping unit of five pixels (0.45 ha) were applied after classification. The maximum likelihood classifier was chosen over machine learning alternatives because it requires no tuning and behaves consistently across dates, which is critical in multi-temporal comparison (Belgiu & Drăguţ, 2016; Talukdar et al., 2020). Accuracy was assessed using 250 stratified random reference points per year, from which overall accuracy, producer's and user's accuracy and the Kappa coefficient were calculated.

### 3.4 Change Detection and Urban Growth Metrics

Post-classification comparison was used to build transition matrices for 2000–2010, 2010–2020, 2020–2024 and 2000–2024, yielding gross gains, losses and from–to conversions. Because the final interval is four years, rates were annualised before comparison. Urban land efficiency was measured by the land consumption rate (built-up area per person) and the land absorption coefficient (new built-up area per additional resident). Growth form was analysed with relative Shannon's entropy across eight 45° directional sectors, concentric distance bands at 2 km intervals from the city centre, road-buffer analysis and Getis-Ord Gi* hotspot analysis on a 500 m grid (Bhat et al., 2017; Chettry & Surawar, 2021).

### 3.5 Environmental Indicators and Predictive Modelling

NDVI was computed from corrected reflectance and grouped into four fixed classes. LST was retrieved from the thermal bands through conversion to radiance and brightness temperature, NDVI-based emissivity estimation and the mono-window algorithm (Sahana et al., 2016). Urban heat island (UHI) intensity was defined as the difference in mean LST between built-up and vegetated land within each scene. Future LULC was simulated with a CA-Markov model that combined Markov transition probabilities with a 5 × 5 contiguity filter and suitability surfaces derived from multi-criteria evaluation and analytic hierarchy process weights (Mishra & Rai, 2016; Tripathy & Kumar, 2019). The model was calibrated on 2010–2020, validated

International Journal for Rapid Research in Engineering Technology & Applied Science (IJRRETAS)

(Peer-Reviewed, Open Access, Fully Refereed International Journal)

Volume 12 issue 02 February 2026 OPEN ACCESS E-ISSN: 2455-4723 Impact Factor 7.95

against the independently classified 2024 map and then recalibrated on 2020–2024 to project 2030, 2035 and 2040 under a business-as-usual scenario. Processing was carried out in ERDAS Imagine, ArcGIS, QGIS, TerrSet and Python.

## 4. Results and Discussion

### 4.1 Classification Accuracy

All four classifications exceeded the commonly accepted 85% accuracy threshold (Table 2). Overall accuracy increased from 86.80% in 2000 to 92.40% in 2024, and Kappa rose from 0.825 to 0.896, placing every year in the almost perfect agreement range. The improvement reflects the superior radiometric quality of the OLI sensors, better reference imagery for recent years and a more spectrally distinct built-up fabric. The main confusion occurred between agricultural and barren land, since harvested fallow fields resemble bare soil in post-monsoon imagery. Because errors compound when two maps are overlaid, the theoretical accuracy of the full-period change map is about 80%, so major conversion pathways are robust whereas small transitions should be read with caution.

**Table 2: Classification accuracy assessment**

| Year | Reference Points | Correctly Classified | Overall Accuracy (%) | Kappa Coefficient |
|---|---|---|---|---|
| 2000 | 250 | 217 | 86.80 | 0.825 |
| 2010 | 250 | 225 | 90.00 | 0.869 |
| 2020 | 250 | 229 | 91.60 | 0.888 |
| 2024 | 250 | 231 | 92.40 | 0.896 |

### 4.2 Land Use/Land Cover Distribution, 2000–2024

The composition of the landscape changed fundamentally over the study period (Table 3; Figure 1). In 2000, agricultural land was the largest category at 84.25 km² (33.70%), followed by vegetation at 72.50 km² (29.00%), and built-up land ranked fourth at 38.75 km² (15.50%). By 2020, built-up land had become the dominant category at 89.60 km² (35.84%), and by 2024 it occupied 100.50 km² or 40.20% of the area. Agricultural land fell to 50.65 km², vegetation dropped below one-fifth of the area to 48.35 km², and water bodies contracted to 9.20 km². Barren and open land remained close to 41–44 km² throughout.

International Journal for Rapid Research in Engineering Technology & Applied Science (IJRRETAS)

(Peer-Reviewed, Open Access, Fully Refereed International Journal)

Volume 12 issue 02 February 2026 OPEN ACCESS E-ISSN: 2455-4723 Impact Factor 7.95

**Table 3: LULC area statistics of Jamshedpur, 2000–2024**

| LULC Class | 2000 (km²) | 2000 (%) | 2010 (km²) | 2010 (%) | 2020 (km²) | 2020 (%) | 2024 (km²) | 2024 (%) |
|---|---|---|---|---|---|---|---|---|
| Built-up | 38.75 | 15.50 | 61.25 | 24.50 | 89.60 | 35.84 | 100.50 | 40.20 |
| Vegetation | 72.50 | 29.00 | 62.30 | 24.92 | 52.15 | 20.86 | 48.35 | 19.34 |
| Agricultural land | 84.25 | 33.70 | 71.45 | 28.58 | 56.30 | 22.52 | 50.65 | 20.26 |
| Water bodies | 12.50 | 5.00 | 11.20 | 4.48 | 9.85 | 3.94 | 9.20 | 3.68 |
| Barren/open land | 42.00 | 16.80 | 43.80 | 17.52 | 42.10 | 16.84 | 41.30 | 16.52 |
| Total | 250.00 | 100.00 | 250.00 | 100.00 | 250.00 | 100.00 | 250.00 | 100.00 |

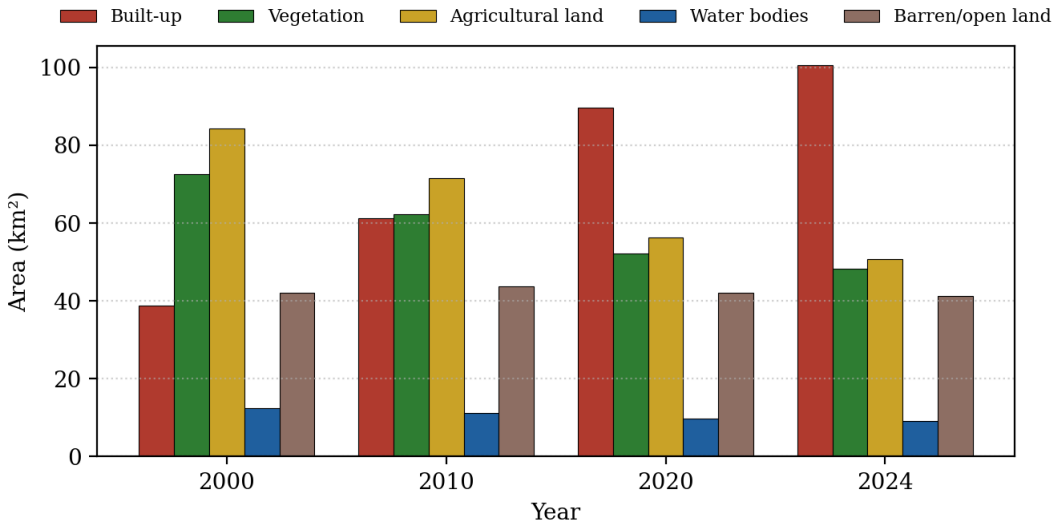


**Figure 1: LULC area distribution of Jamshedpur, 2000–2024**

### 4.3 Magnitude and Rate of Change

Between 2000 and 2024, built-up land gained 61.75 km², an increase of 159.35% and an average of 2.57 km² per year (Table 4). Agricultural land lost 33.60 km² (39.88%), vegetation 24.15 km² (33.31%) and water bodies 3.30 km² (26.40%). The combined losses of these three productive classes (61.05 km²) almost exactly equal the built-up gain, showing that expansion was financed by productive land rather than wasteland. The annual built-up addition rose from 2.25 km² in 2000–2010 to 2.84 km² in 2010–2020 and remained at 2.73 km² in 2020–2024. The compound growth rate fell from 4.68% to 2.91%, but this reflects the enlarged base rather than any easing of pressure. On an annualised proportional basis, agricultural loss accelerated from 2.90% to 3.84% and then 4.13% per year.

International Journal for Rapid Research in Engineering Technology & Applied Science (IJRRETAS)

(Peer-Reviewed, Open Access, Fully Refereed International Journal)

Volume 12 issue 02 February 2026 OPEN ACCESS E-ISSN: 2455-4723 Impact Factor 7.95

**Table 4: LULC change statistics, 2000–2024**

| LULC Class | 2000 (km²) | 2024 (km²) | Change (km²) | Change (%) | Annual Rate (km²/yr) |
|---|---|---|---|---|---|
| Built-up | 38.75 | 100.50 | +61.75 | +159.35 | +2.573 |
| Vegetation | 72.50 | 48.35 | −24.15 | −33.31 | −1.006 |
| Agricultural land | 84.25 | 50.65 | −33.60 | −39.88 | −1.400 |
| Water bodies | 12.50 | 9.20 | −3.30 | −26.40 | −0.138 |
| Barren/open land | 42.00 | 41.30 | −0.70 | −1.67 | −0.029 |

Transition analysis showed that total gross conversion amounted to 96.65 km², or 38.66% of the study area. The largest pathways were agricultural land to built-up (31.20 km²), vegetation to built-up (16.90 km²) and barren to built-up (13.80 km²), which together made up 64.05% of all conversion. Overall, 75.75% of gross built-up gain came directly from agricultural land and vegetation, and this share remained stable in every interval. The near-constant net area of barren land concealed large two-way flows, as farmland and vegetation were cleared and held vacant before construction. Urbanising flows exceeded restorative flows by a ratio of 9.24 to 1, confirming the effective irreversibility of the transformation. These patterns resemble those reported for Ranchi, Dehradun and Bengaluru (Ahmad & Goparaju, 2016; Bhat et al., 2017; Ramachandra et al., 2015).

### 4.4 Pattern and Efficiency of Urban Growth

Urban land expanded much faster than population (Figure 2). Population grew by 59.06% from about 1.10 million to 1.75 million, whereas built-up land grew by 159.35%, giving a ratio of built-up to population compound growth of 2.08. The land consumption rate increased from 35.17 to 57.35 m² per person, and each additional resident was associated with 86–98 m² of new built-up land, well above the average (Table 5). Built-up population density consequently fell by 38.67%, from 28,434 to 17,438 persons per km². A declining land consumption rate ratio (1.303, 1.203 and 1.040) suggests that the inefficiency is moderating but has not been reversed.

International Journal for Rapid Research in Engineering Technology & Applied Science (IJRRETAS)

(Peer-Reviewed, Open Access, Fully Refereed International Journal)

Volume 12 issue 02 February 2026 OPEN ACCESS E-ISSN: 2455-4723 Impact Factor 7.95

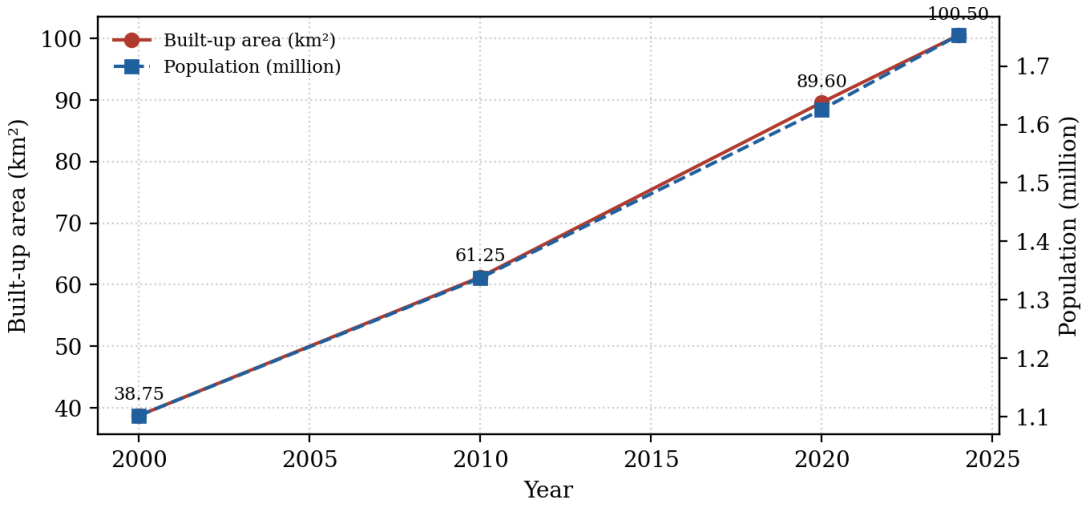


**Figure 2: Built-up area expansion and population growth, 2000–2024**

**Table 5: Urban growth efficiency and dispersion indicators**

| Indicator | 2000 | 2010 | 2020 | 2024 |
|---|---|---|---|---|
| Population | 1,101,800 | 1,337,100 | 1,625,400 | 1,752,500 |
| Land consumption rate (m²/person) | 35.17 | 45.81 | 55.12 | 57.35 |
| Land absorption coefficient (m²/new resident) | — | 95.62 | 98.34 | 85.76 |
| Built-up population density (persons/km²) | 28,434 | 21,830 | 18,141 | 17,438 |
| Relative Shannon's entropy | 0.9843 | 0.9889 | 0.9911 | 0.9918 |

Relative Shannon's entropy was already very high in 2000 (0.9843), reflecting the inherited polycentric structure of the planned township, Adityapur and Mango, and it increased in every period to 0.9918. Every directional sector grew by more than 130%, ranging from 130.43% in the west to 230.77% in the north-east, which indicates the absence of effective directional control. The distance analysis gives the clearest evidence of peripheral growth (Figure 3): the inner 2 km grew by only 26.82%, whereas the 8–10 km band grew by 503.39%, and the two outermost bands absorbed 52.87% of all new built-up land. Road accessibility remained the main locational influence, with 53.48% of built-up land within 1 km of a major road in 2024. Hotspot analysis identified eight significant clusters, led by the NH-33 eastern corridor and the Adityapur industrial belt, which together accounted for 72.39% of built-up gain. Cold spots coincided with reserved forest, floodplain and steep terrain, showing that statutory protection is effective where it exists. These findings agree with the corridor-led, fragmented growth reported for Chennai and the widespread sprawl in mid-sized Indian cities (Aithal & Ramachandra, 2016; Chettry & Surawar, 2021).

International Journal for Rapid Research in Engineering Technology & Applied Science (IJRRETAS)

(Peer-Reviewed, Open Access, Fully Refereed International Journal)

Volume 12 issue 02 February 2026 OPEN ACCESS E-ISSN: 2455-4723 Impact Factor 7.95

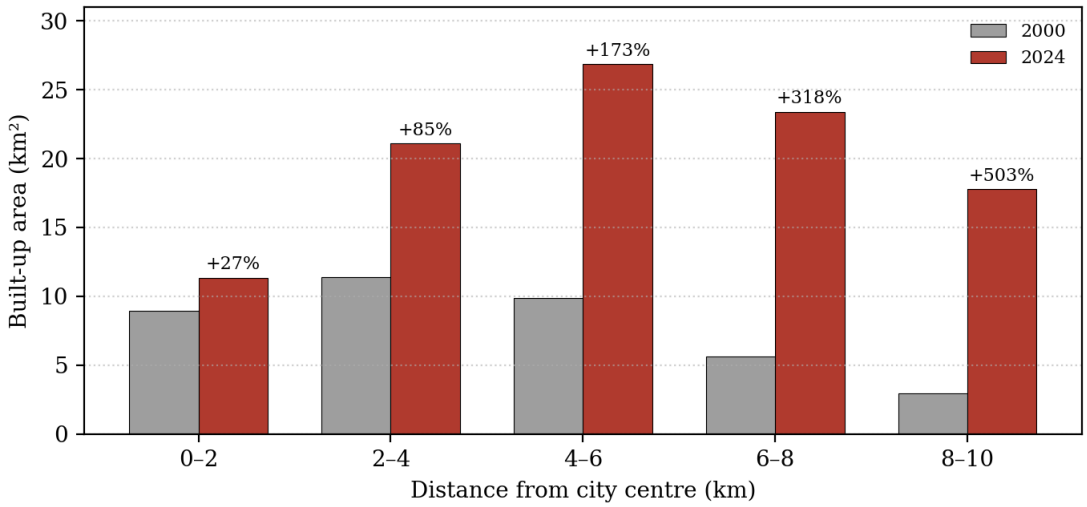


**Figure 3: Built-up area by distance from the city centre, 2000 and 2024**

### 4.5 Environmental Consequences

Vegetation condition deteriorated more severely than the area figures suggest. Mean NDVI fell from 0.412 to 0.268 (34.95%), slightly more than the 33.31% loss of vegetation area. Dense vegetation (NDVI above 0.40) declined from 57.40 to 12.15 km², a loss of 78.83%, while sparse vegetation increased, revealing progressive canopy thinning before conversion. This finding is consistent with the forest degradation documented in Dalma (Ranjan et al., 2016). Surface water declined by 26.40%, with small tanks and ponds losing about three-quarters of their extent, which reduces groundwater recharge and flood attenuation.

Surface temperatures rose for every land cover class (Figure 4), although the absolute rise partly reflects conditions on individual overpass dates. The more robust within-scene measure, UHI intensity, increased from 5.10 °C to 7.40 °C (45.10%), and the built-up–water difference widened from 7.60 °C to 11.20 °C. Vegetation warmed least and continued to provide cooling, while barren land was the hottest surface in every year, reaching 37.00 °C in 2024. This result implies that clearing land long before construction carries a thermal cost. The pattern parallels that reported for Asansol–Durgapur, English Bazar, Chandigarh and Imphal (Choudhury et al., 2019; Mathew et al., 2016; Mondal et al., 2021; Pal & Ziaul, 2017).

International Journal for Rapid Research in Engineering Technology & Applied Science (IJRRETAS)

(Peer-Reviewed, Open Access, Fully Refereed International Journal)

Volume 12 issue 02 February 2026 OPEN ACCESS E-ISSN: 2455-4723 Impact Factor 7.95

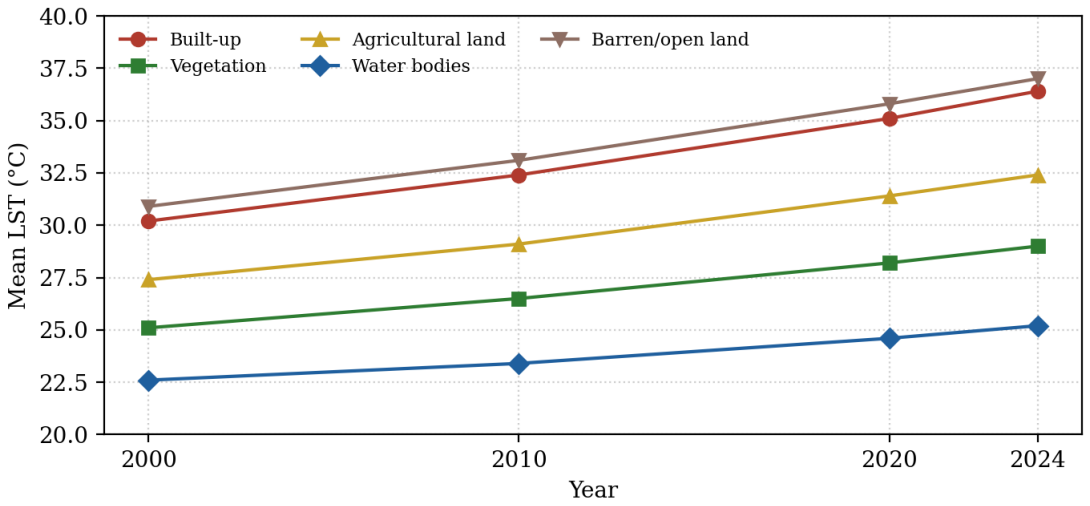


**Figure 4: Mean land surface temperature by LULC class, 2000–2024**

### 4.6 Future LULC Scenario

The CA-Markov model reproduced the 2024 landscape closely, with an overall agreement of 91.20%, Kno of 0.904, Klocation of 0.887 and standard Kappa of 0.869. It underestimated built-up land by 1.74%, which is typical of the stationarity assumption, so the projections represent conservative lower bounds. Under the business-as-usual scenario (Table 6), built-up land would reach 115.80 km² by 2030 and 137.55 km² by 2040, crossing half of the study area around 2035. Agricultural land would fall to 34.35 km² and vegetation to 36.60 km², while water bodies would shrink to 3.00% of the area. Growth would continue to concentrate in the eastern and south-eastern corridors and in the 6–10 km band, in line with modelled trajectories for other Indian cities (Hasnine & Rukhsana, 2020; Tripathy & Kumar, 2019).

**Table 6: CA-Markov predicted LULC scenario (km²)**

| LULC Class | 2024 (Actual) | 2030 | 2035 | 2040 | Share 2040 (%) |
|---|---|---|---|---|---|
| Built-up | 100.50 | 115.80 | 127.30 | 137.55 | 55.02 |
| Vegetation | 48.35 | 43.70 | 40.05 | 36.60 | 14.64 |
| Agricultural land | 50.65 | 43.05 | 38.40 | 34.35 | 13.74 |
| Water bodies | 9.20 | 8.55 | 8.00 | 7.50 | 3.00 |
| Barren/open land | 41.30 | 38.90 | 36.25 | 34.00 | 13.60 |

## 5. Conclusion

This study used multi-temporal Landsat imagery, GIS analysis and predictive modelling to assess urban expansion and LULC change in Jamshedpur from 2000 to 2024. The classifications were reliable, with overall accuracies of 86.80–92.40% and Kappa values of 0.825–0.896. Built-up land expanded by 159.35% and became the dominant land cover, while agricultural land, vegetation and water bodies declined substantially. Three-quarters of new

urban land came directly from farmland and vegetation, and the transformation is effectively irreversible.

Growth was dispersed and peripheral rather than compact. Rising entropy, an increasing land consumption rate, falling built-up density and outer-zone growth more than eighteen times faster than in the core all point to sprawl. The environmental costs are substantial: dense vegetation fell by nearly four-fifths, mean NDVI declined by about 35%, small water bodies largely disappeared and UHI intensity increased by 45%. If current trends continue, more than half of the study area will be built up by 2035.

Several planning implications follow. Density policy offers greater leverage over land consumption than any other instrument, since the 2024 population could have been housed on about 39 km² less land at year-2000 densities. Statutory protection has demonstrably curbed conversion and should be extended to productive agricultural land and to small water bodies. Road investment should be sequenced deliberately because development follows access, and clearance of land should be phased with construction to avoid thermal and hydrological costs. Future research should apply machine learning and higher-resolution imagery, incorporate socio-economic survey data and test alternative policy scenarios to support sustainable, climate-resilient growth in Jamshedpur and similar industrial cities.

**References**

1. Ahmad, F., & Goparaju, L. (2016). Analysis of urban sprawl dynamics using geospatial technology in Ranchi City, Jharkhand, India. Journal of Environmental Geography, 9(1–2), 7–13. https://doi.org/10.1515/jengeo-2016-0002
2. Aithal, B. H., & Ramachandra, T. V. (2016). Visualization of urban growth pattern in Chennai using geoinformatics and spatial metrics. Journal of the Indian Society of Remote Sensing, 44(4), 617–633. https://doi.org/10.1007/s12524-015-0482-0
3. Belgiu, M., & Drăguţ, L. (2016). Random forest in remote sensing: A review of applications and future directions. ISPRS Journal of Photogrammetry and Remote Sensing, 114, 24–31. https://doi.org/10.1016/j.isprsjprs.2016.01.011
4. Bhat, P. A., Shafiq, M., Mir, A. A., & Ahmed, P. (2017). Urban sprawl and its impact on landuse/land cover dynamics of Dehradun City, India. International Journal of Sustainable Built Environment, 6(2), 513–521. https://doi.org/10.1016/j.ijsbe.2017.10.003
5. Chettry, V., & Surawar, M. (2021). Urban sprawl assessment in eight mid-sized Indian cities using RS and GIS. Journal of the Indian Society of Remote Sensing, 49(11), 2721–2740. https://doi.org/10.1007/s12524-021-01420-8
6. Choudhury, D., Das, K., & Das, A. (2019). Assessment of land use land cover changes and its impact on variations of land surface temperature in Asansol-Durgapur Development Region. The Egyptian Journal of Remote Sensing and Space Science, 22(2), 203–218. https://doi.org/10.1016/j.ejrs.2018.05.004
7. Gorelick, N., Hancher, M., Dixon, M., Ilyushchenko, S., Thau, D., & Moore, R. (2017). Google Earth Engine: Planetary-scale geospatial analysis for everyone. Remote Sensing of Environment, 202, 18–27. https://doi.org/10.1016/j.rse.2017.06.031

8. Gu, Z., & Zeng, M. (2024). The use of artificial intelligence and satellite remote sensing in land cover change detection: Review and perspectives. Sustainability, 16(1), Article 274. https://doi.org/10.3390/su16010274
9. Hasnine, M., & Rukhsana. (2020). An analysis of urban sprawl and prediction of future urban town in urban area of developing nation: Case study in India. Journal of the Indian Society of Remote Sensing, 48(6), 909–920. https://doi.org/10.1007/s12524-020-01123-6
10. Mathew, A., Khandelwal, S., & Kaul, N. (2016). Spatial and temporal variations of urban heat island effect and the effect of percentage impervious surface area and elevation on land surface temperature: Study of Chandigarh city, India. Sustainable Cities and Society, 26, 264–277. https://doi.org/10.1016/j.scs.2016.06.018
11. Mishra, V. N., & Rai, P. K. (2016). A remote sensing aided multi-layer perceptron-Markov chain analysis for land use and land cover change prediction in Patna district (Bihar), India. Arabian Journal of Geosciences, 9, Article 249. https://doi.org/10.1007/s12517-015-2138-3
12. Mondal, A., Guha, S., & Kundu, S. (2021). Dynamic status of land surface temperature and spectral indices in Imphal city, India from 1991 to 2021. Geomatics, Natural Hazards and Risk, 12(1), 3265–3286. https://doi.org/10.1080/19475705.2021.2008023
13. Pal, S., & Ziaul, S. (2017). Detection of land use and land cover change and land surface temperature in English Bazar urban centre. The Egyptian Journal of Remote Sensing and Space Science, 20(1), 125–145. https://doi.org/10.1016/j.ejrs.2016.11.003
14. Pandey, A., Mondal, A., & Guha, S. (2024). Assess the relationship of land surface temperature with nine land surface indices in a northeast Indian city using summer and winter Landsat 8 data. Cogent Engineering, 11(1), Article 2382885. https://doi.org/10.1080/23311916.2024.2382885
15. Phiri, D., & Morgenroth, J. (2017). Developments in Landsat land cover classification methods: A review. Remote Sensing, 9(9), Article 967. https://doi.org/10.3390/rs9090967
16. Ramachandra, T. V., Bharath, H. A., & Sowmyashree, M. V. (2015). Monitoring urbanization and its implications in a mega city from space: Spatiotemporal patterns and its indicators. Journal of Environmental Management, 148, 67–81. https://doi.org/10.1016/j.jenvman.2014.02.015
17. Ranjan, A. K., Anand, A., Vallisree, S., & Singh, R. K. (2016). LU/LC change detection and forest degradation analysis in Dalma Wildlife Sanctuary using 3S technology: A case study in Jamshedpur-India. AIMS Geosciences, 2(4), 273–285. https://doi.org/10.3934/geosci.2016.4.273
18. Sahana, M., Ahmed, R., & Sajjad, H. (2016). Analyzing land surface temperature distribution in response to land use/land cover change using split window algorithm and spectral radiance model in Sundarban Biosphere Reserve, India. Modeling Earth Systems and Environment, 2, Article 81. https://doi.org/10.1007/s40808-016-0135-5
19. Talukdar, S., Singha, P., Mahato, S., Shahfahad, Pal, S., Liou, Y.-A., & Rahman, A. (2020). Land-use land-cover classification by machine learning classifiers for satellite observations—A review. Remote Sensing, 12(7), Article 1135. https://doi.org/10.3390/rs12071135
20. Tripathy, P., & Kumar, A. (2019). Monitoring and modelling spatio-temporal urban growth of Delhi using Cellular Automata and geoinformatics. Cities, 90, 52–63. https://doi.org/10.1016/j.cities.2019.01.021